Analytical approach on linear and nonlinear pulse propagations in an open Λ-type molecular system with Doppler broadening

2013 J. Phys. B: At. Mol. Opt. Phys. 46 025103

(http://iopscience.iop.org/0953-4075/46/2/025103)

J. Phys. B: At. Mol. Opt. Phys. **46** (2013) 025103 (11pp) doi:10.1088/0953-4075/46/2/025103

Analytical approach on linear and nonlinear pulse propagations in an open Λ-type molecular system with Doppler broadening

Chaohua Tan, Chengjie Zhu and Guoxiang Huang

State Key Laboratory of Precision Spectroscopy and Department of Physics, East China Normal University, Shanghai 200062, People's Republic of China

E-mail: gxhuang@phy.ecnu.edu.cn

Received 13 September 2012, in final form 3 December 2012
Published 10 January 2013
Online at stacks.iop.org/JPhysB/46/025103

Abstract

We develop a systematic analytical approach on linear and nonlinear pulse propagations in an open Λ-type molecular system with Doppler broadening. In the linear case, using a residue theorem and a spectrum decomposition method, we prove that a crossover from electromagnetically induced transparency (EIT) to Autler–Townes splitting (ATS) exists for a co-propagating configuration of probe and control fields. However, there is no EIT and hence no EIT–ATS crossover for a counter-propagating configuration. We give various explicit formulas, including probe-field spectrum decomposition, the EIT condition, the width of the EIT transparency window, as well as a comparison with the result of cold molecules. Our analytical result agrees well with the experimental one reported recently by Lazoudis *et al* (2010 *Phys. Rev.* A **82** 023812). In the nonlinear case, using the method of multiple scales, we derive a nonlinear envelope equation for probe-field propagation. We show that stable ultraslow solitons can be realized in the open molecular system.

(Some figures may appear in colour only in the online journal)

1. Introduction

In recent years, much attention has been paid to the study of quantum coherent phenomena in various multi-level systems, typical examples include Auter–Townes splitting (ATS) [1] and electromagnetically induced transparency (EIT) [2]. Such phenomena are not only important from the viewpoint of basic research, but also very attractive for many practical applications, such as lasing without inversion, coherent population transfer, enhanced Kerr nonlinearity, slow light, quantum memory, atom and/or photon entanglement, precision spectroscopy, precision measurement, and so on [2, 3].

ATS occurs when the absorption spectrum of a quantum transition can be decomposed into a sum of two net Lorentzian terms if one of the two levels involved in the transition is coupled to a third level induced by a strong control field. EIT occurs when the absorption spectrum can be decomposed not only into two Lorentzians, but also with additional quantum *destructive* interference term(s). Usually, in systems with ATS or EIT, a transparency window is opened. However, the opening of the transparency window cannot tell us whether the phenomenon belongs to ATS or EIT, each of which has a different physical origin. ATS happens only for a strong control field, but EIT happens even when the control field is weak. In particular, only for a weak control field can essential EIT characters be illustrated clearly [4–7].

EIT in various atomic systems has been studied intensively both theoretically and experimentally [2, 3]. However, systematic investigations of EIT in molecular systems are still lacking. To date, there are only several related experimental studies in molecular systems, including the EIT in $^7Li_2$ [8], K_2 [10] and Na_2 vapours [11, 12], in acetylene molecules filled in hollow-core photonic crystal fibres [13, 14] and in photonic microcells [15], and in Cs_2 in a vapour cell [16], and so on. Major difficulties for observing EIT in molecules are small

transition-dipole-moment matrix elements in comparison with those in atoms, and many decay pathways to other molecular states not involved in the main excitation scheme.

In an interesting work reported recently by Lazoudis *et al* [9], EIT in an open hot Λ-type molecular $^7Li_2$ system was studied experimentally. A numerical simulation under a steady-state approximation is used by the authors to solve density matrix equations for molecules. Although the numerical simulation is helpful to explain experimental data, it is however hard to discern ATS from EIT objectively because the physical mechanism behind numerical results are not clear. In particular, since open molecular systems with Doppler broadening are very complicated and have very different features in different parameter regions, it is necessary to clarify, in an analytical way, the quantum interference characters inherent in such systems, which, to the best of our knowledge, has not been done in the literature to date. In addition, it is also necessary to go beyond the steady-state approximation if the probe pulse is used in experiment.

In this work, we develop a systematic analytical approach on linear and nonlinear pulse propagations in open Λ-type molecular systems with Doppler broadening. In the linear case, using the residue theorem and spectrum decomposition method, we prove clearly that an EIT–ATS crossover exists for the co-propagating configuration of probe and control fields. However, there is no EIT and hence no EIT–ATS crossover for the counter-propagating configuration. We provide various explicit formulas, including probe-spectrum decomposition, the EIT condition, and the width of the EIT transparency window, as well as a comparison with the results of cold molecules. Our analytical result agrees well with the experimental one reported recently by Lazoudis *et al* [9]. In the nonlinear case, using the standard method of multiple scales, we derive a nonlinear envelope equation for probe-field propagation. We show that stable ultraslow solitons can be realized in the open molecular system. Notice that nonlinear pulse propagation in coherent atomic systems via EIT has attracted tremendous attention in recent years [17–24], nobody, however, has considered a similar problem for molecules until now.

The paper is arranged as follows. In the next section we present our model and associated Maxwell–Bloch (MB) equations. In section 3, we consider the linear property of the system by using the residue theorem and spectrum decomposition method. Quantum interference characters for hot molecules with both co- and counter-propagating configurations and also for cold molecules are analysed in detail. In section 4, the method of multiple scales is used to study the weak nonlinear propagation of the probe field. Finally, section 5 contains a summary of the main results obtained in our work.

2. The model

The model adopted here is the same as that used in [9]. An open three-state Λ-type Li_2 molecular system (figure 1) consists of an exited upper-level $A^1\Sigma_u^+(v' = 5, J' = 13)$ (labelled $|3\rangle$) and two ground states $X^1\Sigma_g^+(v'' = 1, J'' = 14)$ (labelled $|1\rangle$) and $X^1\Sigma_g^+(v'' = 0, J'' = 12)$ (labelled $|2\rangle$). A control field with centre frequency ω_c couples to the excited state $|3\rangle$ and the ground state $|2\rangle$. The other ground state $|1\rangle$ couples to the $|3\rangle$ by a probe field with centre frequency ω_p. The excited level $|3\rangle$ decays spontaneously to the ground states $|1\rangle$ and $|2\rangle$ with decay rates Γ_{13} and Γ_{23}, respectively. The parameter γ represents the transient relaxation rate of the molecule entering and leaving the interaction region between light and the molecule. It reflects also the additional relaxation of each state due to the interaction with the thermal reservoir [9]. The electric field vector of the system is $\mathbf{E} = \sum_{l=p,c} \mathbf{e}_l \mathcal{E}_l(z,t) e^{i(\mathbf{k}_l \cdot \mathbf{r} - \omega_l t)} + \text{c.c.}$, where $\mathbf{e}_l$ ($\mathbf{k}_l$) is the unit polarization vector (wave number) of the electric field component with the envelope $\mathcal{E}_l$ ($l = p, c$).

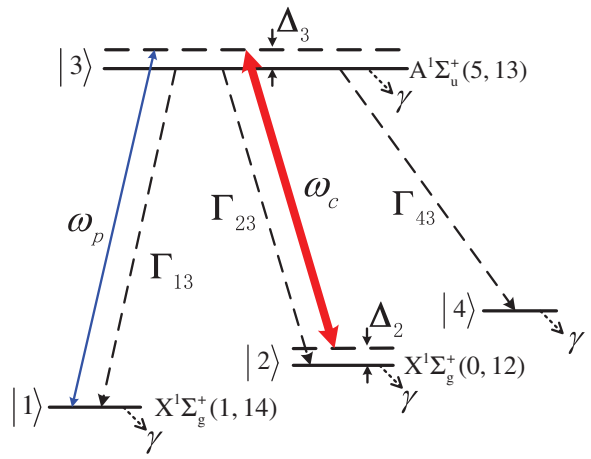

Figure 1. A Λ-type EIT scheme for the open Li_2 molecular system. Excited state $A^1\Sigma_u^+(v' = 5, J' = 13)$ (labelled $|3\rangle$) couples to the ground state $X^1\Sigma_g^+(v'' = 0, J'' = 12)$ (labelled $|2\rangle$) by the control field with centre frequency ω_c and also to another ground state $X^1\Sigma_g^+(v'' = 1, J'' = 14)$ (labelled $|1\rangle$) by the probe field with centre frequency ω_p. Δ_2 and Δ_3 are detunings, Γ_{jl} are population decay rates from $|l\rangle$ to $|j\rangle$, and γ is the transit rate. Molecules occupying the excited state $|3\rangle$ may decay to many other states besides the states $|1\rangle$ and $|2\rangle$. All of these other states are represented by state $|4\rangle$.

As indicated in the last section, decay processes in molecular systems are very complicated in comparison with those of atoms. Many decay pathways to other molecular states not involved in the main excitation scheme exist, and hence the theoretical model considered is necessarily an open one. In the excitation scheme adopted above, molecules occupying the excited level $|3\rangle$ may follow various relaxation pathways and decay to many lower vibration-rotation levels besides the levels $|1\rangle$ and $|2\rangle$. In our modelling all of these levels are represented by the level $|4\rangle$. The decay rate Γ_{43} indicates the spontaneous emission rate of level $|3\rangle$ to level $|4\rangle$ (see figure 1).

For hot molecules, inhomogeneous Doppler broadening must be taken into account because the experiments are carried out in a heat-pipe oven [9]. The Hamiltonian of the system in the interaction picture under electric-dipole and rotating-wave approximations is

$$\hat{H} = -\hbar(\Omega_c e^{i[\mathbf{k}_c \cdot (\mathbf{r}+\mathbf{v}t) - \omega_c t]} |3\rangle\langle 2| + \Omega_p e^{i[\mathbf{k}_p \cdot (\mathbf{r}+\mathbf{v}t) - \omega_p t]} |3\rangle\langle 1| + \text{c.c.}), \quad (1)$$

where $\mathbf{v}$ is molecular velocity, $\Omega_{c(p)} = (\mathbf{e}_{c(p)} \cdot \boldsymbol{\mu}_{32(31)})\,\mathcal{E}_{c(p)}/(2\hbar)$ is half Rabi frequency of the control (probe) field, with $\boldsymbol{\mu}_{jl}$ the electric-dipole matrix element associated with the transition from state $|j\rangle$ to state $|l\rangle$. The optical Bloch equation in the interaction picture reads

$$
\begin{aligned}
&\mathrm{i}\frac{\partial}{\partial t}\sigma_{11} + \mathrm{i}\gamma\left(\sigma_{11} - \sigma_{11}^{\mathrm{eq}}\right) - \mathrm{i}\Gamma_{13}\sigma_{33} + \Omega_p^*\sigma_{31} - \Omega_p\sigma_{31}^* = 0,\\
&\mathrm{i}\frac{\partial}{\partial t}\sigma_{22} + \mathrm{i}\gamma\left(\sigma_{22} - \sigma_{22}^{\mathrm{eq}}\right) - \mathrm{i}\Gamma_{23}\sigma_{33} + \Omega_c^*\sigma_{32} - \Omega_c\sigma_{32}^* = 0,\\
&\mathrm{i}\frac{\partial}{\partial t}\sigma_{33} + \mathrm{i}\gamma\left(\sigma_{33} - \sigma_{33}^{\mathrm{eq}}\right) + \mathrm{i}\Gamma_{3}\sigma_{33} + \Omega_p\sigma_{31}^* + \Omega_c\sigma_{32}^*\\
&\qquad - \Omega_p^*\sigma_{31} - \Omega_c^*\sigma_{32} = 0,\\
&\mathrm{i}\frac{\partial}{\partial t}\sigma_{44} + \mathrm{i}\gamma\left(\sigma_{44} - \sigma_{44}^{\mathrm{eq}}\right) - \mathrm{i}\Gamma_{43}\sigma_{33} = 0,\\
&\left(\mathrm{i}\frac{\partial}{\partial t} + d_{21}\right)\sigma_{21} + \Omega_c^*\sigma_{31} - \Omega_p\sigma_{32}^* = 0,\\
&\left(\mathrm{i}\frac{\partial}{\partial t} + d_{31}\right)\sigma_{31} + \Omega_p(\sigma_{11} - \sigma_{33}) + \Omega_c\sigma_{21} = 0,\\
&\left(\mathrm{i}\frac{\partial}{\partial t} + d_{32}\right)\sigma_{32} + \Omega_c(\sigma_{22} - \sigma_{33}) + \Omega_p\sigma_{21}^* = 0,
\end{aligned}
\tag{2}
$$

for nondiagonal elements, where $d_{21} = -(\mathbf{k}_p - \mathbf{k}_c)\cdot\mathbf{v} + \Delta_2 - \Delta_1 + \mathrm{i}\gamma_{21}$, $d_{31} = -\mathbf{k}_p\cdot\mathbf{v} + \Delta_3 - \Delta_1 + \mathrm{i}\gamma_{31}$, $d_{32} = -\mathbf{k}_c\cdot\mathbf{v} + \Delta_3 - \Delta_2 + \mathrm{i}\gamma_{32}$ with $\gamma_{jl} = (\Gamma_j + \Gamma_l)/2 + \gamma + \gamma_{jl}^{\mathrm{col}}$ $(j, l = 1, 2, 3)$. Here Δ_j $(j = 1, 2, 3)$ are detunings, and Γ_j denotes the total decay rate of the population out of level $|j\rangle$, which is defined by $\Gamma_j = \sum_{l\neq j}\Gamma_{lj}$. The quantity $\gamma_{jl}^{\mathrm{col}}$ is the dephasing rate due to processes such as elastic collisions. $\sigma_{jj}^{\mathrm{eq}}$ is the thermal equilibrium value of σ_{jj} when all electric fields are absent. Equation (2) satisfies $\sum_{j=1}^{4}\sigma_{jj} = 1$ with $\sum_{j=1}^{4}\sigma_{jj}^{\mathrm{eq}} = 1$. At thermal equilibrium, the population in the excited state $|3\rangle$ is much smaller than that of the ground states, i.e. $\sigma_{33}^{\mathrm{eq}} \simeq 0$ and hence $\sigma_{11}^{\mathrm{eq}} + \sigma_{22}^{\mathrm{eq}} + \sigma_{44}^{\mathrm{eq}} \simeq 1$.

The evolution of the electric field is governed by the Maxwell equation. Due to the Doppler effect, the electric polarization intensity of the system is given by $\mathbf{P} = \mathcal{N}_a\int_{-\infty}^{\infty}\mathrm{d}v f(v)\{\boldsymbol{\mu}_{13}\sigma_{31}\exp[\mathrm{i}(k_p z - \omega_p t)] + \boldsymbol{\mu}_{23}\sigma_{32}\exp[\mathrm{i}(k_c z - \omega_c t)] + \mathrm{c.c.}\}$, where $\mathcal{N}_a$ is molecular density and $f(v)$ is the molecular velocity distribution function. For simplicity, we have assumed that electric-field wavevectors are along the z-direction, i.e. $\mathbf{k}_{p,c} = (0, 0, k_{p,c})$. Under the slowly varying envelope approximation, the Maxwell equation reduces to

$$
\mathrm{i}\left(\frac{\partial}{\partial z} + \frac{1}{c}\frac{\partial}{\partial t}\right)\Omega_p + \kappa_{13}\int_{-\infty}^{\infty}\mathrm{d}v f(v)\sigma_{31}(z, v, t) = 0, \tag{3}
$$

with $\kappa_{13} = \mathcal{N}_a\omega_p|\boldsymbol{\mu}_{31}|^2/(2\hbar\varepsilon_0 c)$, here c is the light speed in vacuum.

The MB equations (2) and (3) are our starting point for the study of linear and nonlinear pulse propagations in the open molecular system with Doppler broadening.

3. Linear propagation

3.1. The base state and general linear solution

We first consider linear propagation of the probe field. For this aim, one must know the base state $\sigma_{jl}^{(0)}$, i.e. the steady-state solution of the MB equations (2) and (3) for $\Omega_p = 0$. It is easy to obtain

$$
\begin{aligned}
\sigma_{11}^{(0)} &= \frac{[\gamma\Gamma_{3\gamma}X_1 + (2\gamma + \Gamma_{43})|\Omega_c|^2]\sigma_{11}^{\mathrm{eq}} + \Gamma_{13}|\Omega_c|^2\left(1 - \sigma_{44}^{\mathrm{eq}}\right)}{X_2},\\
\sigma_{22}^{(0)} &= \frac{\gamma[\Gamma_{3\gamma}X_1 + |\Omega_c|^2]\sigma_{22}^{\mathrm{eq}}}{X_2},\\
\sigma_{33}^{(0)} &= \frac{\gamma|\Omega_c|^2\sigma_{22}^{\mathrm{eq}}}{X_2},\\
\sigma_{44}^{(0)} &= \frac{[\gamma\Gamma_{3\gamma}X_1 + (2\gamma + \Gamma_{13})|\Omega_c|^2]\sigma_{44}^{\mathrm{eq}} + \Gamma_{43}|\Omega_c|^2\left(1 - \sigma_{11}^{\mathrm{eq}}\right)}{X_2},\\
\sigma_{32}^{(0)} &= -\frac{\Omega_c}{d_{32}}\cdot\frac{\gamma\Gamma_{3\gamma}X_1\sigma_{22}^{\mathrm{eq}}}{X_2}
\end{aligned}
\tag{4}
$$

and $\sigma_{21}^{(0)} = \sigma_{31}^{(0)} = 0$, where $\Gamma_{3\gamma} \equiv \gamma + \Gamma_3$, $X_1 \equiv \left\{[(\Delta_3 - \Delta_2) - k_c v]^2 + \gamma_{32}^2\right\}/(2\gamma_{32})$ and $X_2 \equiv \gamma(\gamma + \Gamma_3)X_1 + (2\gamma + \Gamma_{13} + \Gamma_{43})|\Omega_c|^2$. Note that in the above expressions $d_{21} = d_{21}(v) = -(k_p - k_c)v + \Delta_2 - \Delta_1 + \mathrm{i}\gamma_{21}$, $d_{31} = d_{31}(v) = -k_p v + \Delta_3 - \Delta_1 + \mathrm{i}\gamma_{31}$, and $d_{32} = d_{32}(v) = -k_c v + \Delta_3 - \Delta_2 + \mathrm{i}\gamma_{32}$.

When switching on the probe field, the base state (4) will be modified. In linear theory, Ω_p is taken as a very small quantity. At first order in Ω_p, the populations and the coherence between states $|2\rangle$ and $|3\rangle$ are not changed, but with

$$
\begin{aligned}
\Omega_p^{(1)} &= F\,\mathrm{e}^{\mathrm{i}\theta},\\
\sigma_{21}^{(1)} &= -\frac{(\omega + d_{31})\sigma_{32}^{*(0)} + \Omega_c^*\left(\sigma_{11}^{(0)} - \sigma_{33}^{(0)}\right)}{|\Omega_c|^2 - (\omega + d_{21})(\omega + d_{31})}F\,\mathrm{e}^{\mathrm{i}\theta}\\
&= a_{21}^{(1)}F\,\mathrm{e}^{\mathrm{i}\theta},\\
\sigma_{31}^{(1)} &= \frac{(\omega + d_{21})\left(\sigma_{11}^{(0)} - \sigma_{33}^{(0)}\right) + \Omega_c\sigma_{32}^{*(0)}}{|\Omega_c|^2 - (\omega + d_{21})(\omega + d_{31})}F\,\mathrm{e}^{\mathrm{i}\theta}\\
&= a_{31}^{(1)}F\,\mathrm{e}^{\mathrm{i}\theta},
\end{aligned}
\tag{5}
$$

where F is a constant, $\theta = K(\omega)z - \omega t$. The linear dispersion relation $K(\omega)$ [1] is given by

$$
K(\omega) = \frac{\omega}{c} + \kappa_{13}\int_{-\infty}^{\infty}\mathrm{d}v f(v) \times\frac{(\omega + d_{21})(\sigma_{11}^{(0)} - \sigma_{33}^{(0)}) + \Omega_c\sigma_{32}^{*(0)}}{|\Omega_c|^2 - (\omega + d_{21})(\omega + d_{31})}. \tag{6}
$$

In thermal equilibrium, $f(v)$ is the Maxwellian velocity distribution function, i.e. $f(v) = 1/(\sqrt{\pi}\,v_T)\exp\left[-v^2/v_T^2\right]$, with $v_T = \sqrt{2k_B T/M}$ the most probable speed at temperature T, and M the molecular mass. The integration in equation (6) with the Maxwellian distribution leads however to some complicated combination of error functions [25], which is very inconvenient for a simple and clear analytical approach. As done by Lee *et al* [26], in the following we use the modified Lorentzian velocity distribution $f(v) = v_T/\left[\sqrt{\pi}\left(v_T^2 + v^2\right)\right]$ to replace the Maxwellian distribution.

We are interested in two different cases: the co-propagating ($k_p \approx k_c$) and counter-propagating configurations ($k_p \approx -k_c$), discussed separately below.

[1] The frequency and wavevector of the probe field are given by $\omega_p + \omega$ and $k_p + K(\omega)$, respectively. Thus $\omega = 0$ corresponds to the centre frequency of the probe field.

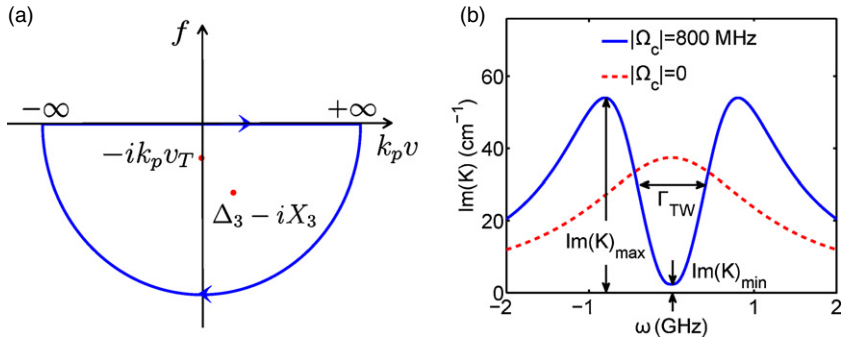

Figure 2. (a) Two poles $(\Delta_2, -iX_3)$, $(0, -ik_p v_T)$ of the integrand in equation (6) in the lower half complex plane. The closed curve with arrows is the contour chosen for calculating the integration in equation (6) using the residue theorem. (b) Absorption spectrum Im(K) as a function of ω for the hot molecular system. The solid (dashed) line for $|\Omega_c| = 800$ MHz ($|\Omega_c| = 0$). Definitions of Im$(K)_{\min}$, Im$(K)_{\max}$, and the width of the transparency window Γ_{TW} are indicated in the figure.

3.2. Hot molecules with the co-propagating configuration

In this configuration, one has $d_{21} = \Delta_2 - \Delta_1 + i\gamma_{21}$, $d_{31} = -k_p v + \Delta_3 - \Delta_1 + i\gamma_{31}$ and $d_{32} = -k_p v + \Delta_3 - \Delta_2 + i\gamma_{32}$. The second term on the right-hand side of equation (6) can be calculated by using the residue theorem [27]. There are two poles in the lower half complex plane

$$k_p v = \Delta_3 - iX_3, \quad k_p v = -ik_p v_T, \tag{7}$$

with $X_3 \equiv \left\{\gamma_{32}^2 + 2\gamma_{32}(2\gamma + \Gamma_{13} + \Gamma_{43})|\Omega_c|^2/[\gamma(\gamma + \Gamma_3)]\right\}^{1/2}$. By taking a contour consisting of a real axis and a semi-circle in the lower half complex plane (see the curves with arrows shown in figure 2(a)), we can calculate the integration in equation (6) analytically by just calculating the residues corresponding to the two poles, and obtain an exact result for the integration. Since the expression is lengthy, we just write down the one with $\Delta_2 = \Delta_3 = 0$, $\Delta\omega_D \gg \gamma_{jl}, \gamma$:

$$\begin{aligned} K &= \frac{\omega}{c} + \mathcal{K}_1 + \mathcal{K}_2, \\ \mathcal{K}_1 &= \frac{\sqrt{\pi}\kappa_{13}\Delta\omega_D[2\gamma_{32}(\omega + i\gamma_{21})A(-iX_3) - iX_3 B]}{\gamma\Gamma_{3\gamma}\left(\Delta\omega_D^2 - X_3^2\right)X_3[|\Omega_c|^2 - (\omega + i\gamma_{21})(\omega + iX_3)]}, \\ \mathcal{K}_2 &= \frac{\sqrt{\pi}\kappa_{13}[2\gamma_{32}(\omega + i\gamma_{21})A(-i\Delta\omega_D) - i\Delta\omega_D B]}{\gamma\Gamma_{3\gamma}\left(X_3^2 - \Delta\omega_D^2\right)[|\Omega_c|^2 - (\omega + i\gamma_{21})(\omega + i\Delta\omega_D)]}, \end{aligned} \tag{8}$$

where $\Delta\omega_D = k_p v_T$ (Doppler width), $A(k_p v) \equiv X_2\sigma_{11}^{(0)} - \gamma|\Omega_c|^2\sigma_{22}^{eq}$ and $B \equiv \gamma\Gamma_{3\gamma}|\Omega_c|^2\sigma_{22}^{eq}$. Note that $\mathcal{K}_1$ ($\mathcal{K}_2$) is contributed by the first (second) pole. For cold molecules, the second pole in equation (7) does not exist, thus $\mathcal{K}_2 = 0$. However, for hot molecules one has $\mathcal{K}_2 \neq 0$ due to the Doppler effect, and hence the system may have very different quantum interference characters compared to that of cold molecules.

In most cases, $K(\omega)$ can be Taylor expanded around the centre frequency of the probe field (corresponding to $\omega = 0$), i.e. $K(\omega) = K_0 + K_1\omega + (1/2)K_2\omega^2 \ldots$, where $K_j \equiv (\partial^j K/\partial\omega^j)_{\omega=0}$. The coefficients K_0 describes the phase shift (real part) and the absorption (imaginary part) per unit length and $1/\mathrm{Re}(K_1)$ and $1/\mathrm{Re}(K_2)$ represent the group velocity v_g and group-velocity dispersion, respectively.

3.2.1. The transparency window of the probe-field absorption spectrum. Im(K) as a function of ω is shown in figure 2(b). The dashed (solid) line is for $|\Omega_c| = 0$ ($|\Omega_c| = 800$ MHz). System parameters are given by $\Gamma_{13} = \Gamma_{23} = \Gamma_{43} = 1.77 \times 10^7$ s^{-1}, $\gamma = 0.47 \times 10^6$ s^{-1}, $\gamma_{jl}^{col} = 4 \times 10^6$ s^{-1}, $\Delta\omega_D = 1.22$ GHz, $\kappa_{13} = 5 \times 10^{10}$ cm^{-1}s^{-1} and $\sigma_{11}^{eq} = \sigma_{22}^{eq} = 0.5$. One sees that the absorption spectrum of the probe field for $|\Omega_c| = 0$ has only a single absorption peak. However, a transparency window opens for a $|\Omega_c = 800$ MHz. The minimum (Im$(K)_{\min}$), maximum (Im$(K)_{\max}$), and width of the transparency window (Γ_{TW}) are defined in the figure.

From equation (8), we obtain the minimum of Im(K) at $\omega = 0$:

$$\mathrm{Im}(K)_{\min} \simeq \frac{\sqrt{\pi}\kappa_{13}}{\Delta\omega_D}\left(\frac{\sigma_{11}^{eq}}{1 + x_1} - \frac{\sigma_{22}^{eq}}{1 + x_1}\frac{1}{1 + \sqrt{x}}\right), \tag{9}$$

where $x \equiv |\Omega_c|^2\gamma_{31}/(\gamma\Delta\omega_D^2)$ and $x_1 \equiv |\Omega_c|^2/(\gamma_{21}\Delta\omega_D)$ are two dimensionless parameters. It is interesting that the system has absorption and gain, reflected by the first and second terms on the right-hand side of equation (9). The gain is due to non-vanishing γ and σ_{22}^{eq}. Obviously, if $x \gg 1$ and $x_1 \gg 1$, i.e. $|\Omega_c|^2\gamma_{31} \gg \gamma\Delta\omega_D^2$ and $|\Omega_c|^2 \gg \gamma_{21}\Delta\omega_D$, one has Im$(K)_{\min} \approx 0$, i.e. a large and deep transparency window in the absorption spectrum is opened. The inequalities can be taken as the EIT condition [16, 26] of the system. When $\gamma_{21} \approx \gamma$, this condition is simplified to $|\Omega_c|^2\gamma_{31} \gg \gamma\Delta\omega_D^2$.

Under the above condition, we obtain $\mathrm{Im}(K)_{\max} \simeq \kappa_{13}\sigma_{11}^{eq}\sqrt{\pi}/\Delta\omega_D$ located at $\omega \approx \pm\Omega_c$, and

$$\Gamma_{TW} \approx 2\left[\frac{2|\Omega_c|^2 + \Delta\omega_D^2 - \Delta\omega_D\sqrt{\Delta\omega_D^2 + 4|\Omega_c|^2}}{2}\right]^{1/2}. \tag{10}$$

3.2.2. EIT–ATS crossover. One of our main purposes is to explicitly analyse the detailed characters of the quantum interference effect of the system, which can be carried out by extending the spectrum decomposition method introduced in [4–7]. Note that $\mathcal{K}_j$ $(j = 1, 2)$ in equation (8) can be decomposed as

$$\mathcal{K}_j = \eta_j\left(\frac{A_{j+}}{\omega - \delta_{j+}} + \frac{A_{j-}}{\omega - \delta_{j-}}\right), \tag{11}$$

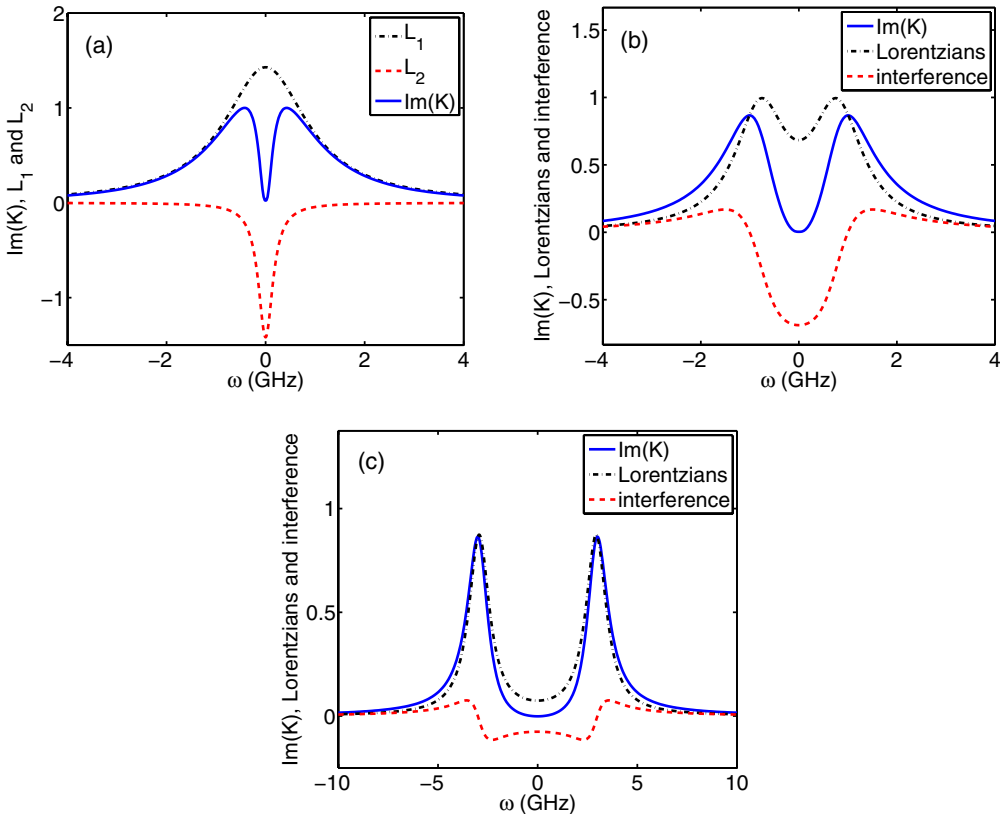

Figure 3. EIT–ATS crossover for hot molecules in the co-propagating configuration. (a) Absorption spectrum in the region $|\Omega_c| < \Omega_{\rm ref} \equiv \Delta\omega_D/2$ contributed by positive L_1 (dashed-dotted line), negative L_2 (dashed line), and total absorption spectrum Im(K) (solid line). (b), (c) Absorption spectrum by two Lorentzians (dashed-dotted line), destructive interference (dashed line), and total absorption spectrum Im(K) (solid line), in the region $|\Omega_c| > \Omega_{\rm ref}$ and $|\Omega_c| \gg \Omega_{\rm ref}$, respectively. Panels (a), (b) and (c) correspond to EIT, EIT–ATS crossover, and ATS, respectively.

where η_j, $A_{j\pm}$ are constants, δ_{j+} and δ_{j-} are two spectrum poles, all of which have been given explicitly in appendix A. From equation (11) we can get explicit expressions of Im($\mathcal{K}_j$) ($j = 1, 2$). However, their general expressions are lengthy and complicated. In order to illustrate the quantum interference effect in a simple and clear way, we decompose Im($\mathcal{K}_j$) according to different regions of Ω_c.

(i) *The weak control field region* (i.e. $|\Omega_c| < \Omega_{\rm ref} \equiv \Delta\omega_D/2$): in this region, one has Re($\delta_{j\pm}$) = 0, Im($A_{j\pm}$) = 0, we obtain

$$\begin{aligned}\mathrm{Im}(K) &= \sum_{j=1}^{2}\mathrm{Im}(\mathcal{K}_j)\\ &= \sum_{j=1}^{2}\eta_j\left(\frac{C_{j+}}{\omega^2+W_{j+}^2}+\frac{C_{j-}}{\omega^2+W_{j-}^2}\right)\\ &= L_1+L_2,\end{aligned} \tag{12}$$

where L_1 and L_2 are defined by

$$\begin{aligned}L_1 &= \frac{\eta_1 C_{1-}}{\omega^2+W_{1-}^2}+\frac{\eta_2 C_{2-}}{\omega^2+W_{2-}^2},\\ L_2 &= \frac{\eta_1 C_{1+}}{\omega^2+W_{1+}^2}+\frac{\eta_2 C_{2+}}{\omega^2+W_{2+}^2},\end{aligned} \tag{13}$$

with real constants

$$\begin{aligned}C_{j+} &= -W_{j+}\left(W_{j+}+\Gamma_j^w\right)/(W_{j+}-W_{j-}),\\ C_{j-} &= W_{j-}\left(W_{j-}+\Gamma_j^w\right)/(W_{j+}-W_{j-}),\\ W_{1\pm} &= \frac{1}{2}[X_3+\gamma_{21}\pm\sqrt{(X_3-\gamma_{21})^2-4|\Omega_c|^2}],\\ W_{2\pm} &= \frac{1}{2}[\Delta\omega_D+\gamma_{21}\pm\sqrt{(\Delta\omega_D-\gamma_{21})^2-4|\Omega_c|^2}],\\ \Gamma_1^w &= \gamma_{21}-\frac{X_3 B}{2\gamma_{32}A(-\mathrm{i}X_3)},\\ \Gamma_2^w &= \gamma_{21}-\frac{\Delta\omega_D B}{2\gamma_{32}A(-\mathrm{i}\Delta\omega_D)}.\end{aligned} \tag{14}$$

Results of L_1, which is a positive single peak (the dashed-dotted line), and L_2, which is a negative single peak (the dashed line) are shown in figure 3(a). System parameters are given by $\Gamma_{13} = \Gamma_{23} = \Gamma_{43} = 1.77 \times 10^7$ s^{-1}, $\gamma = 0.47 \times 10^6$ s^{-1}, $\gamma_{jl}^{\rm col} = 4 \times 10^6$ s^{-1}, $\Delta\omega_D = 1.22$ GHz, and $\Omega_c = 414$ MHz. The sum of the positive L_1 and negative L_2 gives Im(K) (the solid line), which displays an absorption doublet with a significant transparency window near $\omega = 0$. Because a *destructive* interference exists in the probe-field absorption spectrum, the phenomenon found here belongs to EIT according to the criterion given in [5–7].

(ii) *The intermediate control field region* (i.e. $|\Omega_c| > \Omega_{\rm ref}$): by extending the approach by Agarwal [4], we can

decompose $\mathrm{Im}(\mathcal{K}_j)$ $(j = 1, 2)$ as

$$\mathrm{Im}(\mathcal{K}_j) = \eta_j \left\{ \frac{1}{2} \left[\frac{W_j}{(\omega - \delta_j^r)^2 + W_j^2} + \frac{W_j}{(\omega + \delta_j^r)^2 + W_j^2} \right] + \frac{g_j}{2\delta_j^r} \left[\frac{\omega - \delta_j^r}{(\omega - \delta_j^r)^2 + W_j^2} - \frac{\omega + \delta_j^r}{(\omega + \delta_j^r)^2 + W_j^2} \right] \right\}, \tag{15}$$

where

$$\begin{aligned} W_1 &= (\gamma_{21} + X_3)/2, \\ W_2 &= (\gamma_{21} + \Delta\omega_D)/2, \\ \delta_1^r &= \sqrt{4|\Omega_c|^2 - (X_3 - \gamma_{21})^2}/2, \\ \delta_2^r &= \sqrt{4|\Omega_c|^2 - (\Delta\omega_D - \gamma_{21})^2}/2, \\ g_1 &= \frac{X_3 - \gamma_{21}}{2} + \frac{X_3 B}{2\gamma_{32} A(-\mathrm{i}X_3)}, \\ g_2 &= \frac{\Delta\omega_D - \gamma_{21}}{2} + \frac{\Delta\omega_D B}{2\gamma_{32} A(-\mathrm{i}\Delta\omega_D)}. \end{aligned} \tag{16}$$

The first two terms in the first square bracket on the right-hand side of equation (15) are two Lorentzians, resulting from the absorption of two different pathways corresponding to the two dressed states created by the coupling field. The terms in the second square bracket are interference terms, the magnitudes of which are controlled by the parameter g_j. If $g_j > 0$ ($g_j < 0$) the interference is destructive (constructive).

Figure 3(b) shows the result of the probe-field absorption spectrum as functions of ω for $|\Omega_c| > \Omega_{\mathrm{ref}}$. The dashed-dotted line (dashed line) denotes the contribution by two Lorentzians (interference terms). We see that the interference is destructive. The solid line gives the result of $\mathrm{Im}(K)$. System parameters used are the same as those in panel (a) but with $\Omega_c = 1$ GHz. A transparency window opens due to the combined effect of EIT and ATS, which is deeper and wider than that in panel (a). We call such phenomenon the EIT–ATS crossover.

(iii) *The large control field region* (i.e. $|\Omega_c| \gg \Omega_{\mathrm{ref}}$): in this case, the quantum interference strength g_j/δ_j^r in equation (15) is very weak and negligible. We have

$$\mathrm{Im}(\mathcal{K}_j) \approx \frac{\eta_j}{2} \left[\frac{W_j}{(\omega - \delta_j^r)^2 + W_j^2} + \frac{W_j}{(\omega + \delta_j^r)^2 + W_j^2} \right], \tag{17}$$

being the sum of two Lorentzians.

The result of the probe-field absorption spectrum as functions of ω for $|\Omega_c| \gg \Omega_{\mathrm{ref}}$ is shown in figure 3(c). The dashed-dotted line represents the contribution of the sum of the two Lorentzians. For illustration, we have also plotted the contribution from the small interference terms (neglected in equation (17)), denoted by the dashed line. We see that the interference is still destructive but very small. The solid line is the curve of $\mathrm{Im}(K)$, which has two resonances at $\omega \approx \pm\Omega_c$. Parameters used are the same as those in panels (a) and (b) but with $\Omega_c = 3$ GHz. Obviously, the phenomenon found in this situation belongs to ATS because the transparency window opened is mainly due to the contribution of the two Lorenztians.

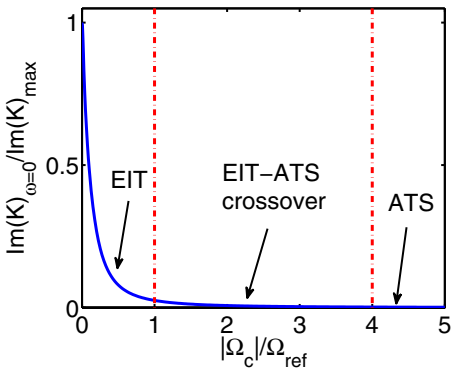

Figure 4. The 'phase diagram' illustrating the transition from EIT to ATS for hot molecules in the co-propagating configuration. $\mathrm{Im}(K)_{\omega=0}/\mathrm{Im}(K)_{\max}$ as a function of $|\Omega_c|/\Omega_{\mathrm{ref}}$ is shown. Three regions (EIT, EIT–ATS crossover and ATS) are divided by two dash-dotted lines.

From the above results, we see that the probe-field absorption spectrum experiences a transition from EIT to ATS as Ω_c is changed from weak to strong values. Since in three-level systems such a phenomenon happens quite often and is universal, we divide quantum interference effects into three classes, i.e. the EIT region ($|\Omega_c| < \Omega_{\mathrm{ref}}$), the region of the EIT–ATS crossover ($1 < |\Omega_c|/\Omega_{\mathrm{ref}} \leqslant 4$), and the ATS region ($|\Omega_c|/\Omega_{\mathrm{ref}} > 4$). Figure 4 shows a 'phase diagram' that illustrates the transition from the EIT to ATS by plotting $\mathrm{Im}(K)_{\omega=0}/\mathrm{Im}(K)_{\max}$ as a function of $|\Omega_c|/\Omega_{\mathrm{ref}}$. Note that we have defined $\mathrm{Im}(K)_{\omega=0}/\mathrm{Im}(K)_{\max} = 0.01$ as the border between EIT–ATS crossover and the ATS regions.

3.2.3. Comparison with experiment. To check the theoretical prediction given above, it is necessary to make a comparison with the experiment reported recently by Lazoudis *et al* [9], which was performed with a co-propagating configuration. Using system parameters $\Gamma_{13} = \Gamma_{23} = \Gamma_{43} = 1.77 \times 10^7$ s^{-1}, $\gamma = 0.47$ MHz, $\gamma_{jl}^{\mathrm{col}} = 4$ MHz, and $\Delta\omega_D = 1.22$ GHz, we have calculated the probe-field absorption spectrum $\mathrm{Im}(K)$ as a function of frequency ω, with $\Omega_c = 414$ MHz (the EIT region) and the control-field detuning -55 MHz. The result is plotted as the dashed line of figure 5, which agrees fairly well with the experimental one (the solid line) measured in [9] (see figure 5(a) of [9]). Note that here we have plotted the quantity $\mathrm{Im}(K)$, which is proportional to fluorescence intensity (measured in [9]) related to the state $|3\rangle$ because $\sigma_{33} \simeq 2|\Omega_p|^2\mathrm{Im}(K)/(\gamma + \Gamma_3)$.[2] The small difference for the depth and width of the EIT dip between our result and the experiment is due to the approximation using the modified Lorentzian distribution to replace the Maxwellian velocity distribution.

[2] Figures 5(b)–(d) in [9] belong to results in the EIT region (i.e. $\Omega_c < \Delta\omega_D/2$) measured for several values of small Ω_c. In general, the smaller the Ω_c, the narrower and shallower the EIT transparency window, which also agree with our theoretical calculation.

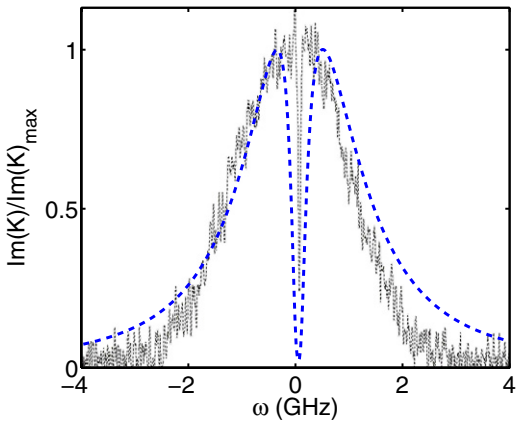

Figure 5. The probe-field absorption spectrum $\mathrm{Im}(K)/\mathrm{Im}(K)_{\max}$ as a function of frequency ω, with $\Omega_c = 414$ MHz (the EIT region). The dashed line is the theoretical result. The solid line is the experimental one reported in [9].

3.3. Hot molecules with a counter-propagating configuration

We now move to the situation when the probe and control fields are arranged as a counter-propagating configuration. Here, $d_{21} = \Delta_2 - \Delta_1 - 2k_p v + \mathrm{i}\gamma_{21}$ and $d_{32} = \Delta_3 - \Delta_2 + k_p v + \mathrm{i}\gamma_{32}$. Then we obtain

$$K = \frac{\omega}{c} + \frac{\kappa_{13}}{\gamma\Gamma_{3\gamma}}(\mathcal{K}_1 + \mathcal{K}_2),$$

$$\mathcal{K}_1 = \frac{\sqrt{\pi}\,\Delta\omega_D[2\gamma_{32}(\omega + \mathrm{i}2X_3)A(-\mathrm{i}X_3) + \mathrm{i}X_3 B]}{(\Delta\omega_D^2 - X_3^2)X_3[|\Omega_c|^2 - (\omega + 2\mathrm{i}X_3)(\omega + \mathrm{i}X_3)]},$$
$$\mathcal{K}_2 = \frac{\sqrt{\pi}[2\gamma_{32}(\omega + \mathrm{i}2\Delta\omega_D)A(-\mathrm{i}\Delta\omega_D) + \mathrm{i}\Delta\omega_D B]}{(X_3^2 - \Delta\omega_D^2)[|\Omega_c|^2 - (\omega + \mathrm{i}2\Delta\omega_D)(\omega + \mathrm{i}\Delta\omega_D)]}, \tag{18}$$

where $\mathcal{K}_1$ and $\mathcal{K}_2$ are obtained from the poles $k_p v = \Delta_3 - \mathrm{i}X_3$ and $k_p v = -\mathrm{i}k_p v_T$, respectively.

We have carried out a similar spectrum decomposition as that performed for the co-propagating configuration given above. To save space, here we omit concrete expressions of the spectrum decomposition but present probe-field absorption spectra in three typical control-field regions in figure 6.

The result of probe-field absorption spectrum $\mathrm{Im}(K)$ in the weak control-field region (i.e. $|\Omega_c| < \Omega_{\mathrm{ref}}$) as a function of ω for $\Omega_c = 500$ MHz is shown in figure 6(a). As in figure 3(a), $\mathrm{Im}(K)$ is also the sum of two terms, i.e. L_1 and L_2. Nevertheless, now both L_1 and L_2 are positive, as illustrated by the dashed-dotted and dashed lines, respectively. We see that $\mathrm{Im}(K)$ (the solid line) displays only a positive single peak, there is no transparency window, and the reason is that the quantum interference becomes constructive (the red dashed line) for the counter-propagating configuration. Thus, different from the case of the co-propagating configuration, in the weak control-field region, an EIT, which we have defined as the transparency window plus a destructive interference, does not exist.

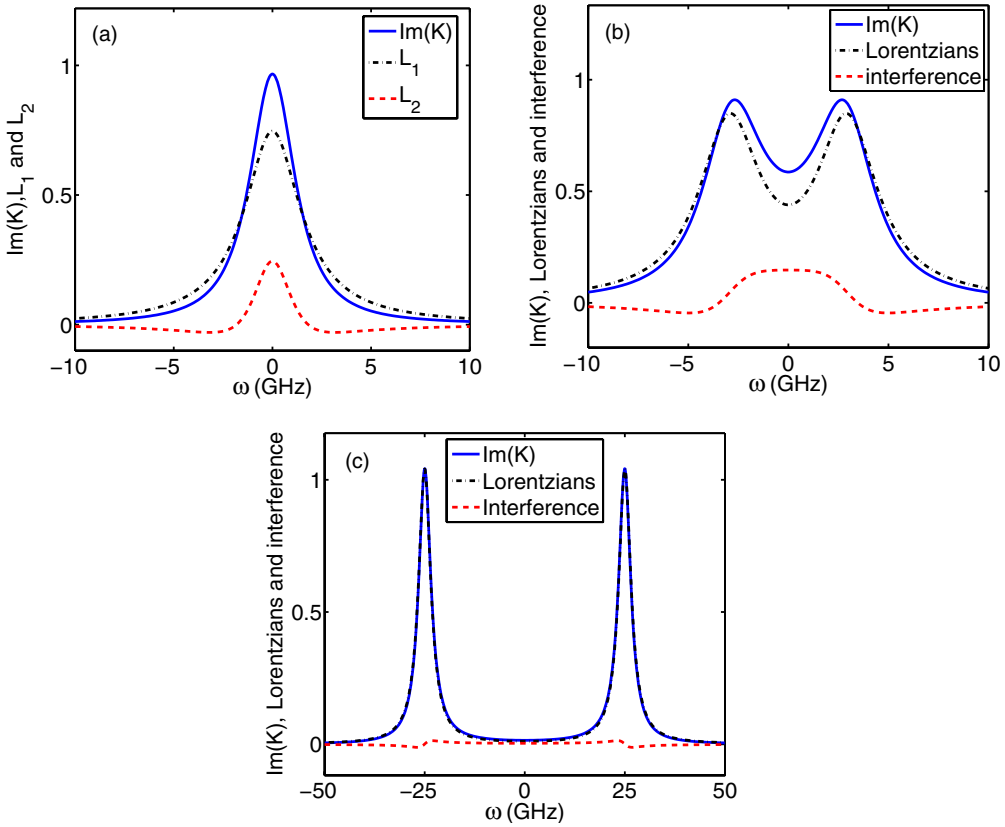

Figure 6. Probe-field absorption spectrum for hot molecules in the counter-propagating configuration. (a) Absorption spectrum in the region $|\Omega_c| < \Omega_{\mathrm{ref}} \equiv \Delta\omega_D/2$ contributed by positive L_1 (dashed-dotted line) and L_2 (dashed line), and the total absorption spectrum $\mathrm{Im}(K)$ (solid line). (b), (c) Absorption spectrum by two Lorentzians (dashed-dotted line), constructive interference (dashed line) and total absorption spectrum $\mathrm{Im}(K)$ (solid line), in the region $|\Omega_c| > \Omega_{\mathrm{ref}}$ and $|\Omega_c| \gg \Omega_{\mathrm{ref}}$, respectively.

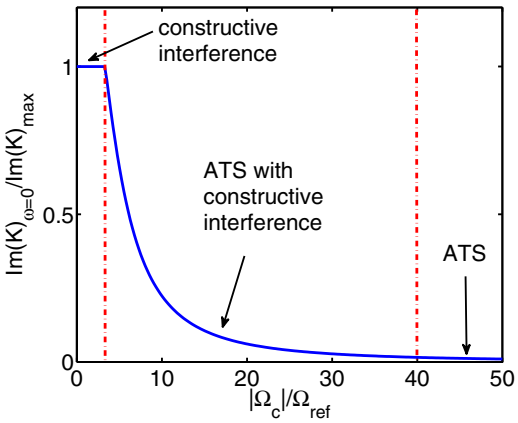

Figure 7. $\mathrm{Im}(K)_{\omega=0}/\mathrm{Im}(K)_{\max}$ as a function of the control field $|\Omega_c|/\Omega_{\mathrm{ref}}$ for hot molecules in the counter-propagating configuration. Three regions (constructive interference, ATS with constructive interference and ATS) are divided by two dashed-dotted lines.

Results of the probe-field absorption spectra as functions of ω for $|\Omega_c| > \Omega_{\mathrm{ref}}$ and $|\Omega_c| \gg \Omega_{\mathrm{ref}}$, respectively, are shown in figures 6(b) and (c). System parameters are given by $\Gamma_{13} = \Gamma_{23} = \Gamma_{43} = 1.77 \times 10^7\ \mathrm{s}^{-1}$, $\gamma = 0.47 \times 10^6\ \mathrm{s}^{-1}$, $\gamma_{ij}^{\mathrm{col}} = 4 \times 10^6\ \mathrm{s}^{-1}$, and $\Delta\omega_D = 1.22$ GHz, with $\Omega_c = 3$ GHz (in the intermediate control-field region) and $\Omega_c = 25$ GHz (in the large control-field region) for panel (b) and panel (c), respectively. The dashed-dotted line (dashed line) denotes the contribution by the sum of two Lorentzians terms (interference terms) in $\mathrm{Im}(K)$. The solid line gives the result of $\mathrm{Im}(K)$. We see that the interferences near the probe-field centre frequency (i.e. $\omega = 0$) are always constructive. Consequently, different from the case of the co-propagating configuration, no EIT–ATS crossover happens.

The 'phase diagram' that illustrates the transition from the constructive interference to ATS for the counter-propagating configuration by plotting $\mathrm{Im}(K)_{\omega=0}/\mathrm{Im}(K)_{\max}$ as a function of $|\Omega_c|/\Omega_{\mathrm{ref}}$ is shown in figure 7. Three regions are divided as constructive interference, ATS with constructive interference, and ATS, respectively.

3.4. Cold molecules and comparison for various cases

Our model presented in section 2 is also valid for cold molecules. In this case, one should take $v = 0$ in the Bloch equation (2), and $f(v) = \delta(v)$ in the Maxwell equation (3). The solutions (4) and (5) are still valid but one must take $v = 0$ there. However, the dispersion relation (6) is replaced by

$$K(\omega) = \frac{\omega}{c} + \frac{\kappa_{13}\left(\sigma_{11}^{(0)} - \sigma_{33}^{(0)}\right)(\omega + \mathrm{i}\Gamma)}{|\Omega_c|^2 - (\omega + \mathrm{i}\gamma_{21})(\omega + \mathrm{i}\gamma_{31})}, \tag{19}$$

with $\Gamma = \gamma_{21} + |\Omega_c|^2\left(\sigma_{33}^{(0)} - \sigma_{22}^{(0)}\right)/\left[\gamma_{32}\left(\sigma_{11}^{(0)} - \sigma_{33}^{(0)}\right)\right]$. Here $\Delta_2 = \Delta_3 = 0$ has been taken for simplicity.

A similar spectrum decomposition can be performed like that done for hot molecules, which is omitted here.

The probe-field absorption spectrum $\mathrm{Im}(K)_{\omega=0}/\mathrm{Im}(K)_{\max}$ as a function of the control field $|\Omega_c|/\Omega_{\mathrm{ref}}$, where $\Omega_{\mathrm{ref}} \equiv |\gamma_{21} - \gamma_{31}|/2$ is shown in figure 8. System parameters are given by $\Gamma_{13} = \Gamma_{23} = \Gamma_{43} = 1.77 \times 10^7\ \mathrm{s}^{-1}$, $\gamma_{ij}^{\mathrm{col}} =$

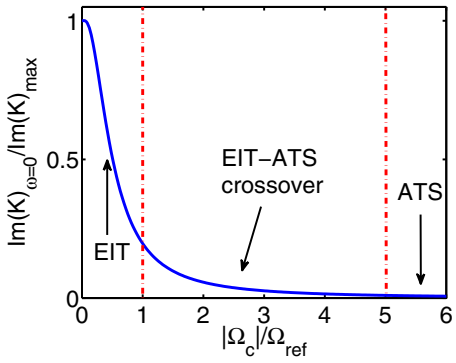

Figure 8. Transition from EIT to ATS for cold molecules. $\mathrm{Im}(K)_{\omega=0}/\mathrm{Im}(K)_{\max}$ as a function of $|\Omega_c|/\Omega_{\mathrm{ref}}$ is shown, where $\Omega_{\mathrm{ref}} \equiv |\gamma_{21} - \gamma_{31}|/2$. Three regions (EIT, EI–ATS crossover and ATS) are divided by two dash-dotted lines.

$1 \times 10^3\ \mathrm{s}^{-1}$ and $\sigma_{11}^{\mathrm{eq}} = 1$. From the figure, we obtain a similar conclusion as that obtained for the co-propagation configuration, i.e. the probe-field absorption spectrum also experiences a transition from EIT to ATS as Ω_c is increased. The quantum interference effect in the system can be divided into three regions, i.e. the EIT region ($|\Omega_c| < \Omega_{\mathrm{ref}}$), the region of the EIT–ATS crossover ($1 < |\Omega_c|/\Omega_{\mathrm{ref}} \leqslant 5$), and the ATS region ($|\Omega_c|/\Omega_{\mathrm{ref}} > 5$).

From the results given above, we see that the quantum coherence in the open Λ-type molecular system has very interesting features, depending on the existence or non-existence of the Doppler broadening, and also depending on the beam propagating (co-propagating or counter-propagating) configurations. For comparison, in table 1 some useful physical quantities, including the EIT condition, absorption spectrum $\mathrm{Im}(K)|_{\omega=0}$, group velocity v_g, and the width of the transparency window Γ_{TW}, are presented for several different physical cases.

The first line in the table is for hot molecules working in the co-propagating configuration; the second line is for hot molecules working in the counter-propagating configuration; the third line is for cold molecules. There are EIT, EIT–ATS crossover, and ATS for both cold molecules and the hot molecules with the co-propagating configuration. But there is no EIT and no EIT–ATS crossover for the hot molecules with the counter-propagating configuration. Experimentally, to date only the EIT in the co-propagating configuration has been demonstrated recently by experiment [9].

4. Nonlinear pulse propagation

The theoretical approach given in the last two sections is valid not only for continuous-wave but also for pulsed probe fields. However, if the probe field is pulsed and has a larger amplitude, the nonlinear effect induced by Kerr nonlinearity inherent in the system must be taken into account. We stress that the theoretical scheme proposed in the present work is very suitable for the study of pulse propagation in multi-level systems.

In this section, we investigate nonlinear pulse propagation, especially ultraslow optical solitons, in the present open hot

Table 1. Propagating properties of the probe field for various open Λ-type molecular systems, including the EIT condition, absorption spectrum $\mathrm{Im}(K)|_{\omega=0}$, width of the transparency window Γ_{TW}, and group velocity v_g for three different cases. Other quantities appearing in the table have been defined in the text. Mol.=Molecules, Co-prop.=Co-propagating configuration, Cou.-prop.=Counter-propagating configuration.

System	EIT condition	$\mathrm{Im}(K)\|_{\omega=0}$	Γ_{TW}	v_g
Hot mol. (co-prop.)	$\frac{\gamma\Delta\omega_D^2}{\gamma_{31}} \leqslant \|\Omega_c\|^2 \leqslant \frac{(\Delta\omega_D)^2}{4}$	$\frac{\sqrt{\pi}\kappa_{13}\gamma_{21}}{\|\Omega_c\|^2}$	$\frac{2\|\Omega_c\|^2}{\Delta\omega_D}$	$\frac{\|\Omega_c\|^2}{\sqrt{\pi}\kappa_{13}}$
Hot mol. (cou.-prop.)	No EIT	$\frac{\sqrt{\pi}\kappa_{13}\Delta\omega_D}{\|\Omega_c\|^2}$	$2\|\Omega_c\| - \Delta\omega_D$	$\frac{\|\Omega_c\|^2}{\sqrt{\pi}\kappa_{13}}$
Cold mol.	$\gamma_{21}\gamma_{31} \leqslant \|\Omega_c\|^2 \leqslant \frac{\gamma_{31}^2}{4}$	$\frac{\kappa_{13}\gamma_{21}}{\|\Omega_c\|^2}$	$\frac{2\|\Omega_c\|^2}{\gamma_{31}}$	$\frac{\|\Omega_c\|^2}{\kappa_{13}}$

molecular system with co-propagating configuration using the method of multiple scales. To achieve this aim, we take the asymptotic expansion $\sigma_{jl} - \sigma_{jl}^{(0)} = \sum_{m=1,2,\ldots} \epsilon^m \sigma_{jl}^{(m)}$, $\Omega_p = \sum_{m=1,2,\ldots} \epsilon^m \Omega_p^{(m)}$, with $\sigma_{jj}^{(1)} = 0$ and $\sigma_{32}^{(1)} = 0$, where ϵ is a small parameter denoting the typical amplitude of Ω_p and all quantities on the right-hand side of the asymptotic expansion are considered as functions of the multi-scale variables $z_m = \epsilon^m z$ $(m = 0, 1, 2)$, $t_m = \epsilon^m t$ $(m = 0, 1)$. Substituting the expansion into the MB equations (2) and (3), we obtain a series of linear but inhomogeneous equations for $\sigma_{ij}^{(m)}$ and $\Omega_p^{(m)}$ $(m = 1{-}4)$, which can be solved order by order.

The zeroth-order $(m = 0)$ and the first-order $(m = 1)$ solutions are the same as that given respectively by equation (4) and (5), by now $\theta = K(\omega)z_0 - \omega t_0$ and F is the yet to be determined envelope function of the 'slow' variables t_1, z_1 and z_2. In the second order $(m = 2)$, a divergence-free solution for $\Omega_p^{(2)}$ requires the solvability condition $\mathrm{i}[\partial F/\partial z_1 + (\partial K/\partial\omega)\partial F/\partial t_1] = 0$, which shows that the envelope function F travels with complex group velocity $(\partial K/\partial\omega)^{-1}$. Explicit expressions of the second order solution have been given in appendix B.

In the third order $(m = 3)$, the Kerr nonlinearity of the system plays a role. A divergence-free solution for $\Omega_p^{(3)}$ gives rise to the equation

$$\mathrm{i}\frac{\partial F}{\partial z_2} - \frac{1}{2}\frac{\partial^2 K}{\partial\omega^2}\frac{\partial^2 F}{\partial t_1^2} - W|F|^2 F\mathrm{e}^{-2\bar{\alpha}z_2} = 0, \tag{20}$$

where $\alpha = \mathrm{Im}(K) = \epsilon^2\bar{\alpha}$ and

$$W = -\kappa_{13}\int_{-\infty}^{\infty}\mathrm{d}v f(v)\frac{\Omega_c a_{32}^{*(2)} + (\omega + d_{21})\left(a_{11}^{(2)} - a_{33}^{(2)}\right)}{|\Omega_c|^2 - (\omega + d_{21})(\omega + d_{31})}, \tag{21}$$

with coefficients $a_{11}^{(2)}$, $a_{22}^{(2)}$ and $a_{32}^{(2)}$ are defined in appendix B.

Combining equation (20) and the solvability condition in the second order, we obtain

$$\mathrm{i}\frac{\partial}{\partial z}U - \frac{1}{2}\frac{\partial^2 K}{\partial\omega^2}\frac{\partial^2 U}{\partial\tau^2} - W|U|^2 U\mathrm{e}^{-2\alpha z} = 0, \tag{22}$$

where $\tau = t - z/v_g$ and $U = \epsilon F$. Equation (22) is a nonlinear Schrödinger (NLS) equation describing the time evolution of the envelope function F, in which W is proportional to third-order nonlinear susceptibility (the Kerr coefficient) relevant to self-phase modulation, which is necessary for the formation of a shape-preserved probe pulse.

The key for the formation and propagation of an optical soliton in the system requires two conditions. The first is a balance between dispersion and nonlinearity, and the second is the absorption of the probe field must be negligibly small. Generally, the coefficients of equation (22) are complex, which means that a soliton, even if it is produced initially, may be highly unstable during propagation. However, as shown below, a realistic set of system parameters can be found under the EIT condition so that the imaginary part of these coefficients can be made much smaller than their corresponding real part. Thus it is possible to get a shape-preserving nonlinear localized solution that can propagate a rather long distance without a significant distortion.

Neglecting the small imaginary part of the coefficients and taking $\omega = 0$, equation (22) can be written in the dimensionless form $\mathrm{i}\partial u/\partial s + \partial^2 u/\partial\sigma^2 + 2|u|^2 u = 0$, with $s = -z/(2L_D)$, $\sigma = \tau/\tau_0$, and $u = U/U_0$. Here τ_0 is the typical pulse duration, $L_D = \tau_0^2/\widetilde{K}_2$ is the typical dispersion length, and $U_0 = (1/\tau_0)\sqrt{\widetilde{K}_2/\widetilde{W}}$ is the typical half Rabi frequency of the probe field, with $\widetilde{K}_2$ and $\widetilde{W}$ being the real part of $K_2 = (\partial^2 K/\partial\omega^2)_{\omega=0}$ and $W|_{\omega=0}$, respectively. Then one can obtain various soliton solutions for u. A single-soliton solution in terms of the half Rabi frequency reads

$$\Omega_p = \frac{1}{\tau_0}\sqrt{\frac{\widetilde{K}_2}{\widetilde{W}}}\,\mathrm{sech}\left(\frac{t}{\tau_0} - \frac{z}{\tau_0 v_g}\right)\exp\left[\mathrm{i}\left(\widetilde{K}_0 + \frac{1}{2L_D}\right)z\right] \tag{23}$$

with $\widetilde{K}_0 = \mathrm{Re}(K)|_{\omega=0}$, which describes a bright soliton travelling with the propagating velocity $v_g = [\mathrm{Re}(\partial K/\partial\omega)]^{-1}|_{\omega=0}$.

We now give a realistic parameter set for the formation of the optical soliton given above. For a hot Li_2 molecular gas, we choose $\Omega_c = 600$ MHz, $\Delta_2 = \Delta_3 \approx 2.36 \times 10^7$ s^{-1}, $\tau_0 = 1.0 \times 10^{-7}$ s, $\omega_p = 4.46 \times 10^{14}$ s^{-1}, and other parameters are the same as those given in the previous text. Then we obtain $K_2 = (5.51 + 0.672i) \times 10^{-16}$ cm^{-1}s^2 and $W = (1.75 + 0.298\mathrm{i}) \times 10^{-16}$ cm^{-1}s^2, $L_D = L_{NL} = 18.2$ cm, and $U_0 = 1.77 \times 10^7$ s^{-1}. One sees that the imaginary part of K_2 and W is indeed much smaller than their corresponding real part. The reason of so small an imaginary part is due to the quantum interference effect contributed by the control field.

The propagating velocity of the probe pulse can be estimated by the real part of the linear dispersion relation (6). At the probe-field centre frequency (i.e. $\omega = 0$) we obtain $v_g = [\mathrm{Re}(\partial K/\partial\omega)|_{\omega=0}]^{-1} \approx 2.13 \times 10^{-4}c$. Consequently, the optical soliton obtained may travel with an ultraslow propagating velocity in the system.

The stability of the ultraslow optical soliton described above can be checked by using numerical simulations. In

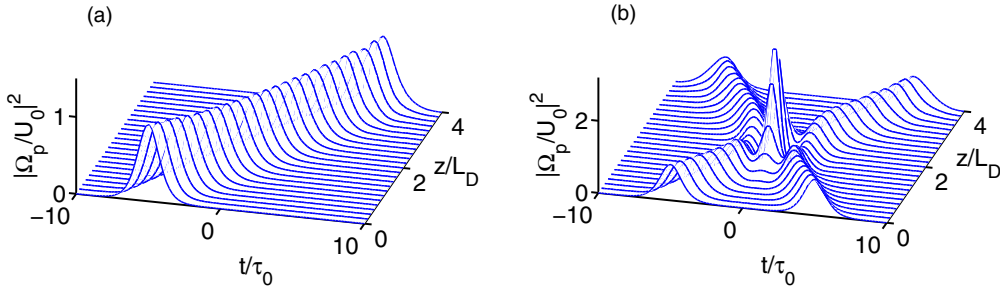

Figure 9. (a) Ultraslow optical solitons and their interaction in the hot molecular system. (a) Three-dimensional plot of the waveshape of $|\Omega_p/U_0|^2$ as a function of z/L_D and t/τ_0. (b) Collision between two ultraslow optical solitons.

figure 9(a), we show the wave shape of $|\Omega_p/U_0|^2$ as a function of z/L_D and t/τ_0. The solution is obtained by numerically solving equation (22) with full complex coefficients included. The initial condition is given by $\Omega_p(0,t) = U_0\mathrm{sech}(t/\tau_0)$. We see that the amplitude of the soliton undergoes only a slight decrease and its width undergoes a slight increase due to the influence of the imaginary part of the coefficients. A simulation of the interaction between two ultraslow optical solitons is also carried out by inputting two identical solitons (see figure 9(b)). The initial condition is $\Omega_p(0,t) = U_0\mathrm{sech}(t/\tau_0 - 5) + U_0\mathrm{sech}(t/\tau_0 + 5)$. As time goes on, they collide, pass through, and depart from each other. The two solitons recover their initial waveforms after the collision. However, a phase shift is observed after the collision.

5. Conclusion

We have developed a systematic analytical approach on linear and nonlinear pulse propagations in an open Λ-type molecular system with Doppler broadening. In the linear case, using the residue theorem and spectrum decomposition method, we have proved that a crossover exists from EIT to ATS for the co-propagating configuration. However, there is no EIT and hence no EIT–ATS crossover for the counter-propagating configuration. We have provided various explicit formulas, including probe-field spectrum decomposition, the EIT condition, and width of the EIT transparency window, as well as a comparison with the result of cold molecules. Our analytical result agrees well with the experimental one reported recently by Lazoudis *et al* [9]. In the nonlinear case, using the method of multiple scales, we have derived a nonlinear envelope equation for probe-field propagation. We show that stable ultraslow solitons can be realized in the open molecular system. New theoretical predictions presented in this work are helpful for guiding new experimental findings in coherent molecular systems and may have promising practical applications in coherent molecular spectroscopy, precision measurement, molecular quantum state control, nonlinear pulse propagation, and so on.

Acknowledgments

This work was supported by NSF-China under grant numbers 10874043 and 11174080.

Appendix A. Expressions of η_j, $A_{j\pm}$, and $\delta_{j\pm}$

$$\eta_1 = \frac{\kappa_{13}\sqrt{\pi}\gamma_{32}\Delta\omega_D A(-\mathrm{i}X_3)}{\gamma\Gamma_{3\gamma}X_3\left(\Delta\omega_D^2 - X_3^2\right)}, \tag{A.1}$$

$$\eta_2 = \frac{\kappa_{13}\sqrt{\pi}\gamma_{32}A(-\mathrm{i}\Delta\omega_D)}{\gamma\Gamma_{3\gamma}\left(X_3^2 - \Delta\omega_D^2\right)}, \tag{A.2}$$

$$\delta_{1\pm} = \frac{1}{2}[-\mathrm{i}(X_3 + \gamma_{21}) \pm \sqrt{4|\Omega_c|^2 - (X_3 - \gamma_{21})^2}], \tag{A.3}$$

$$\delta_{2\pm} = \frac{1}{2}[-\mathrm{i}(\Delta\omega_D + \gamma_{21}) \pm \sqrt{4|\Omega_c|^2 - (\Delta\omega_D - \gamma_{21})^2}], \tag{A.4}$$

$$A_{1\pm} = \mp\frac{\delta_{1\pm} - \left[\gamma_{21} - \frac{X_3 B}{2\gamma_{32}A(-\mathrm{i}X_3)}\right]}{\delta_{1+} - \delta_{1-}}, \tag{A.5}$$

$$A_{2\pm} = \mp\frac{\delta_{2\pm} - \left[\gamma_{21} - \frac{\Delta\omega_D B}{2\gamma_{32}A(-\mathrm{i}\Delta\omega_D)}\right]}{\delta_{2+} - \delta_{2-}}. \tag{A.6}$$

Appendix B. Second-order solution of MB equations

$$\begin{aligned}\sigma_{21}^{(2)} &= \frac{\mathrm{i}}{D}\left[(\omega + d_{31})a_{21}^{(1)} - \Omega_c^* a_{31}^{(1)}\right]\frac{\partial F}{\partial t_1}\mathrm{e}^{\mathrm{i}\theta} \\ &= a_{21}^{(2)}\frac{\partial F}{\partial t_1}\mathrm{e}^{\mathrm{i}\theta},\end{aligned} \tag{B.1}$$

$$\begin{aligned}\sigma_{31}^{(2)} &= \frac{\mathrm{i}}{D}\left[(\omega + d_{21})a_{31}^{(1)} - \Omega_c a_{21}^{(1)}\right]\frac{\partial F}{\partial t_1}\mathrm{e}^{\mathrm{i}\theta} \\ &= a_{31}^{(2)}\frac{\partial F}{\partial t_1}\mathrm{e}^{\mathrm{i}\theta},\end{aligned} \tag{B.2}$$

$$\begin{aligned}\sigma_{33}^{(2)} &= \frac{\mathrm{i}}{D_1}\left\{[\gamma^2(\omega + d_{32})(\omega + d_{32}^*) + 2\gamma\gamma_{32}|\Omega_c|^2]\right. \\ &\quad \times \left(a_{31}^{*(1)} - a_{31}^{(1)}\right) - \gamma(\gamma + \Gamma_{31})\left[\Omega_c a_{21}^{(1)}(\omega + d_{32})\right. \\ &\quad \left.\left. - \Omega_c^* a_{21}^{*(1)}(\omega + d_{32}^*)\right]\right\}|F|^2\,\mathrm{e}^{-2\tilde{\alpha}z_2} \\ &= a_{33}^{(2)}|F|^2\,\mathrm{e}^{-2\tilde{\alpha}z_2},\end{aligned} \tag{B.3}$$

$$\begin{aligned}\sigma_{11}^{(2)} &= \left[\frac{\Gamma_{13}}{\gamma + \Gamma_{31}}a_{33}^{(2)} - \frac{\mathrm{i}}{\gamma + \Gamma_{31}}\left(a_{31}^{*(1)} - a_{31}^{(1)}\right)\right]|F|^2\,\mathrm{e}^{-2\tilde{\alpha}z_2} \\ &= a_{11}^{(2)}|F|^2\,\mathrm{e}^{-2\tilde{\alpha}z_2},\end{aligned} \tag{B.4}$$

$$\sigma_{22}^{(2)} = -\left(\sigma_{11}^{(2)} + \sigma_{33}^{(2)} + \sigma_{44}^{(2)}\right) = a_{22}^{(2)}|F|^2\,\mathrm{e}^{-2\bar{\alpha}z_2}, \tag{B.5}$$

$$\sigma_{44}^{(2)} = \frac{\Gamma_{43}}{\gamma}a_{33}^{(2)}|F|^2\,\mathrm{e}^{-2\bar{\alpha}z_2} = a_{44}^{(2)}|F|^2\,\mathrm{e}^{-2\bar{\alpha}z_2}, \tag{B.6}$$

$$\begin{aligned}\sigma_{32}^{(2)} &= \left[\frac{\Omega_c}{\omega + d_{32}}\left(a_{33}^{(2)} - a_{22}^{(2)}\right) - \frac{a_{21}^{*(1)}}{\omega + d_{32}}\right]|F|^2\,\mathrm{e}^{-2\bar{\alpha}z_2} \\ &= a_{32}^{(2)}|F|^2\,\mathrm{e}^{-2\bar{\alpha}z_2},\end{aligned} \tag{B.7}$$

with $D \equiv |\Omega_c|^2 - (\omega + d_{21})(\omega + d_{31})$ and $D_1 \equiv \gamma[(\gamma + \Gamma_{23} + \Gamma_{43})(\gamma + \Gamma_{31}) + \gamma\Gamma_{13}](\omega + d_{32})\left(\omega + d_{32}^*\right) + 2\gamma_{32}[(2\gamma + \Gamma_{43})(\gamma + \Gamma_{31}) + \gamma\Gamma_{13}]|\Omega_c|^2$. $a_{21}^{(1)}$ and $a_{31}^{(1)}$ have been defined in equation (5).

References

[1] Autler S R and Townes C R 1955 *Phys. Rev.* **100** 703
[2] Fleischhauer M, Imamoglu A and Marangos J P 2005 *Rev. Mod. Phys.* **77** 633
[3] Khurgin K B and Tucker R S (ed) 2009 *Slow Light: Science and Applications* (Boca Raton, FL: Taylor and Francis)
[4] Agarwal G S 1997 *Phys. Rev.* A **55** 2467
[5] Anisimov P and Kocharovskaya O 2008 *J. Mod. Opt.* **55** 3159
[6] Abi-Salloum T Y 2010 *Phys. Rev.* A **81** 053836
[7] Anisimov P M, Dowling J P and Sanders B C 2011 *Phys. Rev. Lett.* **107** 163604
[8] Qi J, Spano F C, Kirova T, Lazoudis A, Magnes J, Li L, Narducci L M, Field R W and Lyyra A M 2002 *Phys. Rev. Lett.* **88** 173003
[9] Lazoudis A, Kirova T, Ahmed E H, Li L, Qi J and Lyyra A M 2010 *Phys. Rev. A.* **82** 023812
[10] Li L, Qi P, Lazoudis A, Ahmed E and Lyyra A M 2005 *Chem. Phys. Lett.* **403** 262
[11] Lazoudis A, Ahmed E H, Li L, Kirova T, Qi P, Hansson A, Magnes J and Lyyra A M 2008 *Phys. Rev.* A **78** 043405
[12] Lazoudis A, Kirova T, Ahmed E H, Qi P, Huennekens J and Lyyra A M 2011 *Phys. Rev.* A **83** 063419
[13] Ghosh S, Sharping J E, Ouzounov D G and Gaeta A L 2005 *Phys. Rev. Lett.* **94** 093902
[14] Benabid F and Roberts P J 2011 *J. Mod. Opt.* **58** 87
[15] Light P S, Benabid F, Pearce G J, Couny F and Bird D M 2009 *Appl. Phys. Lett.* **94** 141103
[16] Li H, Chen H, Gubin M A, Rostovtsev Y V, Sautenkov V A and Scully M O 2010 *Laser Phys.* **20** 1725
[17] Hong T 2003 *Phys. Rev. Lett.* **90** 183901
[18] Wu Y and Deng L 2004 *Phys. Rev. Lett.* **93** 143904
[19] Huang G, Deng L and Payne M G 2005 *Phys. Rev.* E **72** 016617
[20] Hang C, Huang G and Deng L 2006 *Phys. Rev.* E **73** 036607
[21] Michinel H, Paz-Alonso M J and Perez-Garcia V M 2006 *Phys. Rev. Lett.* **96** 023903
[22] Huang G, Hang C and Deng L 2008 *Phys. Rev.* A **77** 011803
[23] Yang W-X, Chen A-X, Si L-G, Jiang K, Yang X and Lee R-K 2010 *Phys. Rev.* A **81** 023814
[24] Li L and Huang G 2010 *Phys. Rev.* A **82** 023809
[25] Ahmed E H and Lyyra A M 2007 *Phys. Rev.* A **76** 053407
[26] Lee H, Rostovtsev Y, Bednar C J and Javan A 2003 *Appl. Phys.* B **76** 33–9
[27] Byron F W and Fuller R W 1992 *Mathematics of Classical and Quantum Physics* chapter 6 (New York: Dover)